Journal of Colloid and Interface Science 405 (2013) 256–261

Contents lists available at SciVerse ScienceDirect

Journal of Colloid and Interface Science

www.elsevier.com/locate/jcis

Disassembly of redox responsive poly(ferrocenylsilane) multilayers: The effect of blocking layers, supporting electrolyte and polyion molar mass

Jing Song [a], Dominik Jańczewski [a], Yujie Ma [b], Mark Hempenius [c], Jianwei Xu [a,*], G. Julius Vancso [c,*]

[a] Institute of Materials Research and Engineering, A*STAR (Agency for Science, Technology and Research), 3 Research Link, Singapore 117602, Singapore
[b] Institute for Molecules and Materials, Radboud University Nijmegen, Heyendaalseweg 135, 6525 AJ Nijmegen, The Netherlands
[c] MESA+ Institute for Nanotechnology, Materials Science and Technology of Polymers, University of Twente, P.O. Box 217, 7500 AE Enschede, The Netherlands

ARTICLE INFO

Article history:
Received 11 January 2013
Accepted 2 May 2013
Available online 17 May 2013

Keywords:
Layer by layer
Redox response
Disassembly
Multilayer
Organometallic polymer

ABSTRACT

Layer by layer (LbL) organometallic multilayers, composed of poly(ferrocenylsilane) (PFS) polycations and polyanions, were fabricated and characterized. Disassembly of redox responsive PFS^-/PFS^+ films as well as multilayers consisting of PFS^-/PFS^+ combined with redox inert bilayers was studied. The influence of parameters on disassembly kinetics and mechanism, such as distance between redox PFS multilayers and the electrode, effect of the top inert layer, the choice of the supporting electrolyte, the ionic strength of the solution, and the molar mass of polymers, was investigated. The results elucidate the details of the disassembly mechanism and provide design criteria for preparing templates with highly controllable disassembly kinetics.

1. Introduction

Compared to other stimuli, such as pH, temperature, or light, the use of redox potential, to address "smart" polymers, offers distinct advantages. Redox potentials can be controlled in an easy and precise way and can also be employed to provide spatial control over domains with dimensions as thick as the thinnest conducting wires that can be obtained by nanofabrication (i.e., on the order of 10–20 nm) [1]. In addition to many applications as for example, mechanical actuators or sensors, redox responsive polymers can also act as a molecular release medium with tuneable release properties [2,3]. Such macromolecules can act as reservoirs for an active therapeutic cargo in form of thin films (polymer brushes, multilayer films, membranes) [4,5] or submicron particles (micelles, nanogels, capsules, mesoporous particles and vesicles) [6–8]. Among the listed structures, layer by layer (LbL) thin films are particularly versatile and suitable for incorporation of multiple functional or responsive components with controlled morphology, thickness, and film composition [9,10]. Fabrication of redox responsive LbL films combines the advantages of nanoscale electrochemical features with an easy processing, high control over the morphology, and tuneable functionality which is amenable to, e.g., medical delivery applications.

Poly(ferrocenylsilane) (PFS) is a unique organometallic polymer, exhibiting alternating ferrocene and silane units within the main chain [11–13]. Since reversible redox processes affect the ferrocene group within its backbone, PFS is undergoing dramatic and reversible changes in physicochemical properties upon oxidation. Protocols for preparation of PFS polymers, with additional positive and negative charges [14], make those macromolecules suitable for a LbL fabrication.

Only few polymers lend themselves for a construction of active LbL redox responsive release systems. Kwon et al. reported on an electroactive polymeric system, which rapidly changes from a solid state to solution in response to small electric currents, achieving modulated release of insulin [15]. The Hammond group presented remotely controlled release of precise quantities of chemical agents from Prussian Blue (PB) composite multilayers [16]. Recently, electrochemically tailored degradation of polyelectrolyte assemblies was described by Zambelli, and coworkers [17]. Degradation of engineered LbL capsules upon exposure to a cellular concentration of glutathione was also presented [18]. Despite the studies aiming at the assembly and disassembly, as well as controlled molecular release from LbL prepared PFS films [8,14,19–21], no systematic exploration was performed on various important aspects of electrochemically induced molecular behavior of PFS multilayers. Such a study would be indispensable for the design of smart platforms for molecular delivery applications.

In our recent communication, we reported on a redox responsive LbL system constructed with PFS polyelectrolytes, with

* Corresponding authors. Fax: +65 68720785 (J. Xu), +31 53 4893823 (G.J. Vancso).
E-mail addresses: songj@imre.a-star.edu.sg (J. Song), janczewskid@imre.a-star.edu.sg (D. Jańczewski), Y.Ma@science.ru.nl (Y. Ma), M.A.Hempenius@utwente.nl (M. Hempenius), jw-xu@imre.a-star.edu.sg (J. Xu), g.j.vancso@utwente.nl (G.J. Vancso).

0021-9797/$ - see front matter © 2013 Elsevier Inc. All rights reserved.
http://dx.doi.org/10.1016/j.jcis.2013.05.008

particular focus on disassembly of films and release of guest molecules upon oxidation [22]. In the present contribution, we provide an enhanced mechanistic study of LbL PFS multilayer disassembly in the context of various external parameters like presence of blocking layers, ionic strength of electrolyte, counterion, and molar mass of the PFS influence. Oxidation potential shifts, electron transfer mechanisms and ion diffusion processes, phenomena related to the redox active film behavior, are also discussed. In-depth understanding of undergoing processes provides a set of tools to construct complex delivery systems and to host drug release profiles in a pre-programmed manner, in a real-time response to physiological changes.

2. Experiment

2.1. Materials

Poly(ethyleneimine) (PEI, $M_w \sim 2.5 \times 10^4$ g/mol), poly(styrene sulfonate) (PSS, $M_w \sim 7.0 \times 10^4$ g/mol), poly(acrylic acid) (PAA, $M_w \sim 4.5 \times 10^5$ g/mol), poly(allylamine hydrochloride) (PAH, $M_w \sim 5.6 \times 10^4$ g/mol), 3-aminopropyltrimethoxysilane, sodium chloride, sodium nitride, sodium perchlorate, and sodium sulfate were obtained from Aldrich and used as received.

2.2. PFS synthesis

Positively and negatively charged PFSs with $M_w = 1.67 \times 10^4$ g/mol, PDI = 1.3; $M_w = 5.3 \times 10^4$ g/mol, PDI = 1.3; and $M_w = 2.5 \times 10^5$ g/mol, PDI = 2.7 were synthesized by ROP of chlorinated cycloferrocenophane followed by the side group modification as described previously [23].

2.3. Multilayer fabrication

Multilayers were deposited on Indium Tin Oxide (ITO)-glass or ITO-Quartz substrates (Ssens, the Netherlands), which were cleaned in advance by immersing them into a mixture of H_2O, H_2O_2, and NH_4OH with a volume ratio of 5:1:1 for 20 min., followed by extensive rinsing with MilliQ water and drying under nitrogen stream. The cleaned ITO substrates were first immersed in a toluene solution of 3-aminopropyltrimethoxysilane (0.1 mM) to impart positive charges onto the surface. The modified substrates were alternatively immersed in the polycation and polyanion aqueous solutions (1 mg/ml, 0.5 M NaCl) for 10 min with rinsing, dipping into pure MiliQ water and drying with a stream of nitrogen gas. Different types of composite multilayers were fabricated.

2.4. Characterization

UV/Vis spectra were recorded on a Varian Cary 300 Bio instrument in double beam mode using an uncovered quartz slide as a reference. Cyclic voltammetry measurements were carried out on an Autolab PGSTAT 10 (Ecochemie, Utrecht, the Netherlands) potentiostat in a three-electrode configuration. The ITO substrates acted as the working electrode, Ag/AgCl as the reference electrode, and Pt as the counter electrode. Different electrolyte solutions including ($NaClO_4$, NaCl, $NaNO_3$, and Na_2SO_4) were used. Prior to the measurements, the electrochemical cell was degassed by passing nitrogen through the electrolyte solution for 5 min. A series of cyclic voltammograms were recorded after holding the oxidation potentials at different values for different time intervals. The amount of transferred charge Q was calculated based on the integration of the area under each cyclic voltammogram. The film disassembly was monitored by CV or in situ electrochemical UV/Vis as described in [22]. For in situ electrochemical UV/Vis cell configuration, see supplementary data.

3. Results and discussion

LbL assemblies composed of positively charged PFS^+ and negatively charged PFS^- polyelectrolytes were fabricated using materials and methods previously reported by our group [21,22] (Scheme 1a and b). The thickness development during fabrication of the multilayer on ITO and Au coated glass substrates was monitored by cyclic voltammetry (CV), ellipsometry, quartz microbalance (QCM), and UV/Vis spectroscopy [14,20–22]. PFS multilayers exhibit linear growth with an average thickness increase of 3 nm/bilayer on ITO substrate in dry state. The linear increase in CV's peak current versus scan rate suggested that all electroactive material within the multilayers is addressed during the electrochemical cycle. Upon oxidation of the PFS multilayers, the oxidation and the reduction currents decrease owing to a dissolution of the film deposited on the electrode [22].

3.1. Blocking effect

For composite multilayers, with a short separation distance between redox active species and the electrode, e.g., mixed poly(styrene sulfonate) and poly(ferrocenylsilane) $(PSS^-/PFS^+)_5$, the electroactivity of the PFS layer is clearly observable [22]. Charge transport mechanism within LbL for such cases was discussed by the group of Schlenoff and Laurent [24]. In the present study, the tailored designed PFS composite multilayers provided the opportunity to evaluate the distance dependence of electron transfer from the electrode to the redox active materials.

In order to assess the role of blocking films at the electrode surface, electroactive $(PFS^-/PFS^+)_3$ bilayers were fabricated on top of the redox inactive spacer. Poly(acrylic acid) (PAA^-) and poly(allylamine hydrochloride) (PAH^+), were deposited in form of $(PAA^-/PAH^+)_n$ multilayers, as a bottom inert blocking film ($n = 1$–5), (Scheme 1c). Samples with increasing numbers of $(PAA^-/PAH^+)_n$ layers were subjected to the cyclic voltammetry in 0.1 M $NaClO_4$ as shown in Fig. 1a. The shape of the cyclic voltammogram is effected by the single bilayer, $(PAA^-/PAH^+)_1$ showing an increase in the separation of the cathodic and anodic peaks, respectively. This refers to a decrease in the rate constants for electron transfer due to build up of an insulating barrier separating the redox pair from the electrode. Fig. 1b shows the charge passed for oxidation/reduction of ferrocene as a function of the number of electrochemically inactive double layer number, as determined by the integration of the areas under the redox peaks. Deposition of two blocking layers decreases the current by nearly 97% and four blocking layers terminate detectable redox activity. The approximate threshold distance to prevent redox events in our system is 9 nm corresponding to 3 bilayers. This behavior also confirms earlier conclusions that there are no salt counterions in the multilayers. Our observations are in agreement with Schlenoff et al., who considered the blocking effect of PSS^-/PAH^+ layers on electrochemically active viologen containing polyions [24]. They found that in LbL films, the redox active material interpenetrated into the blocking inert parts of the film for a distance of approximately 2.5 bilayers. We note that such interpenetration of polyelectrolytes has also been confirmed by neutron reflectivity [25].

Moser et al. in earlier work considered electron transfer in proteins assuming tunneling [26]. The maximum distance the electron can tunnel is a few angstroms, and the rate of electron transfer k follows the relationship [27,28] $k = k_0 \exp[-\beta R]$, where β is the decay constant, on the order of 1 $Å^{-1}$ and R is the distance between donor and acceptor sites or between electrode and electroactive species. In this cited study, the value of electron rate constant falls from ca. 10^{13} s^{-1} to 10^0 s^{-1} from contact to 2.5 nm separation, respectively. This value is smaller but still within the bulk part of

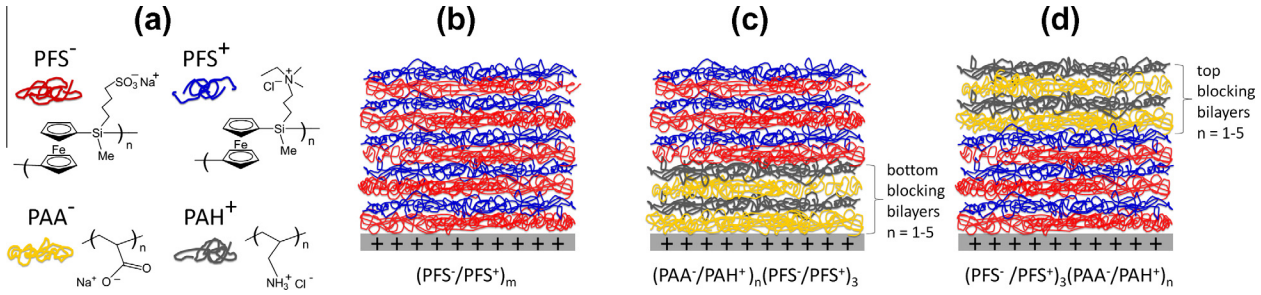

Scheme 1. Schematic representation of LbL structures. (a) Polyelectrolytes used in experiments, (b) typical structure of (PFS^-/PFS^+) multilayers, (c) film configuration for experiments with bottom blocking layers and (d) film configuration for experiments with top blocking layers.

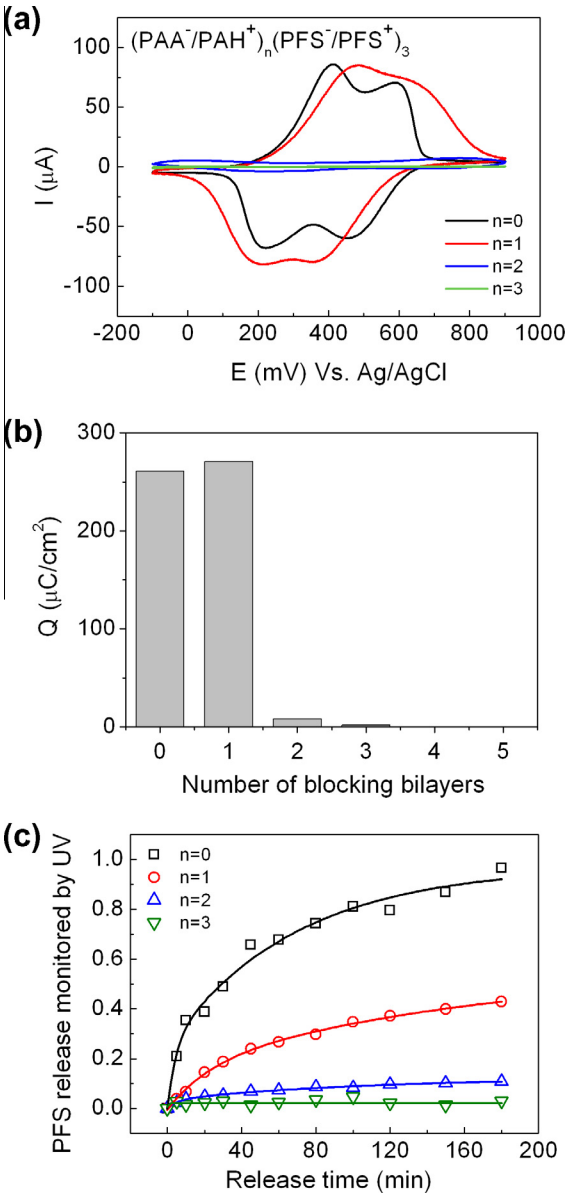

Fig. 1. (a) Cyclic voltammograms of a $(PFS^-/PFS^+)_3$ bilayers separated from the electrode by non-electrochemical $(PAA^-/PAH^+)_n$ bilayers, $n = 1–5$. Supporting electrolyte, 0.1 M $NaClO_4$, scan rate, 50 mV/s. (b) Total addressable charges passed for the oxidation/reduction of ferrocene as a function of blocking bilayer number. (c) Disassembly profile of multicomponent multilayers, monitored by UV.

the observed threshold cutoff for the multilayer studied here. Yet in view of the statistical nature of segmental arrangements in LbL multilayers and the corresponding averaging, no definitive conclusions can be made based on this distance comparison regarding conductivity mechanisms.

Composite multilayer disassembly for films including bottom blocking layer was monitored by in situ electrochemical-UV/Vis spectroscopy (Fig. 1c), (see supplementary data). PFS release at elevated oxidation potentials was observed only for systems which included less than three blocking layers. Above the threshold of 9 nm in blocking layer thickness ($n = 3$), the films were stable, indicating lack of the oxidation process. Thus, the use of blocking layers provides an additional tool to engineer PFS (and guest) release profiles from PFS^-/PFS^+ multilayers.

As described by the Gibbs–Donnan equilibrium, when the redox state of the active sites in the film is changed, counterions in the supporting electrolyte have a trend to diffuse into the multilayer to compensate for the missing charges [29]. Apart from the electrostatic repulsion of charged polymeric domains, this effect additionally contributes to the osmotic pressure and may also cause the polyelectrolyte multilayers to disassembly as we discussed in a previous paper [22]. To evaluate electrochemical blocking effects of redox inactive polyelectrolytes layers deposited on top of PFS multilayers, an inactive outer $(PAA^-/PAH^+)_n$ system was employed (Scheme 1d). Fig. 2a shows the typical cyclic voltammogram of multicomponent polyelectrolytes $(PFS^-/PFS^+)_3(PAA^-/PAH^+)_n$ for $n = 1–5$. The shape of the cyclic voltammogram slightly changed after deposition of the $(PAA^-/PAH^+)_n$ layer on the top, and the cathodic and anodic peak separation increased by 24 mV. This may be related to the interpenetration of the inactive polymer chain or different surface charge. There are no large differences between the cyclic voltammograms observed with an increasing blocking layer thickness. The total addressable redox charge was kept constant with increasing the top blocking layer number (Fig. 2b). The PFS multilayer disassembly profile shows similar trend and no visible influence of outer blocking layers on the film disassembly kinetics (Fig. 2c).

During a redox process, counterion fluxes are driven by electrostatic forces. According to the presented evidence, the top inactive layer number from 1 to 5 is not providing sufficient barrier for perchlorate anion migration. Oxidation profiles and PFS release rates are not affected by presence of top blocking layers.

3.2. Ionic strength effect

To investigate the effect of the supporting electrolyte ionic strength on the multilayer disassembly, PFS multilayers were exposed to solutions with different concentrations of $NaClO_4$. Fig. 3a shows typical cyclic voltammograms of a $(PFS^-/PFS^+)_5$ bilayer structure in various salt concentrations. The *I–E* curves do not display any change in the total charge of the redox process (the area under the redox curve). However, upon decrease in the ionic strength of the solution, the position of the redox peak is visibly shifted to higher potentials. Table I (see supplementary data)

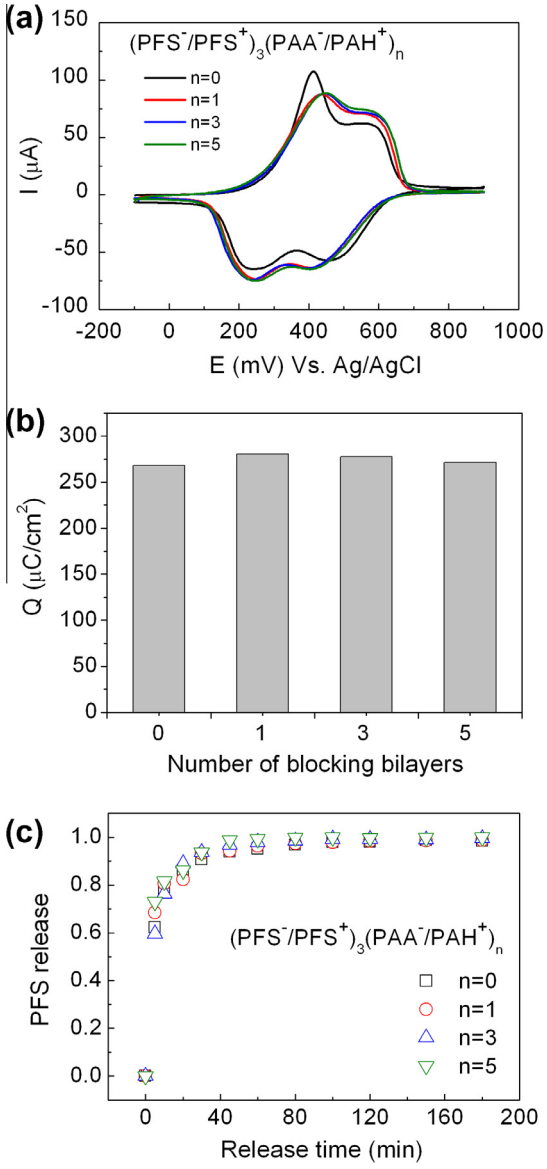

Fig. 2. (a) Cyclic voltammograms of $(PFS^-/PFS^+)_3(PAA^-/PAH^+)_n$ bilayers, $n = 1$–5. Supporting electrolyte, 0.1 M $NaClO_4$, scan rate, 50 mV/s. (b) Total addressable charges passed for the oxidation/reduction of ferrocene as a function of blocking layer number. (c) Disassembly profile of multicomponent multilayers.

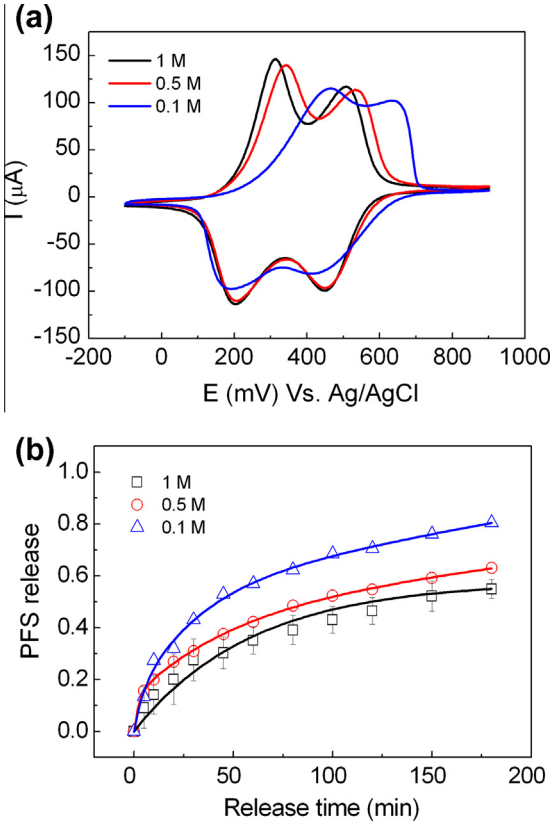

Fig. 3. (a) Typical cyclic voltammograms recorded on a $(PFS^-/PFS^+)_5$ multilayer assembled on ITO electrode at different concentration of $NaClO_4$ electrolyte solutions. (b) $(PFS^-/PFS^+)_5$ dissemble rate at 0.9 V (vs. Ag/AgCl) oxidation potential as a function of accumulated holding time at the different ionic strength of $NaClO_4$ electrolyte, (□) 1 M, (○) 0.5 M, (Δ) 0.1 M.

shows the measured values of the redox peak potential in solutions with different ionic strengths. This effect observed can be explained by the Donnan potential. The Donnan potential of polyelectrolyte multilayers is related to the number of fixed charges in the film [29]. The top layer of the multilayer structure possesses additional charge present at the surface. As a result of charge overcompensation, the multilayers grow [30,31]. Negative and positive ζ potentials, $\zeta = \pm 60$ mV, were observed for PFS^- and for PFS^+, respectively [32]. $\Delta\varnothing_D$, the interfacial Donnan potential, is related to the fixed charges on the film surface and the ionic strength of the electrolyte as given by Eq. (1) [29] and is changing the observable potential as presented by Eq. (2).

$$\Delta\varnothing \approx \omega \frac{RT}{F} \ln \frac{c_F}{c_S} \tag{1}$$

$$E = E_0 + \Delta\varnothing_D \tag{2}$$

where c_s is the 1:1 electrolyte concentration (e.g., sodium chloride) in the external solution, c_F is the concentration of fixed charged sites in the polymer, and ω is the ionic charge of the fixed ionic sites in the polymer. The Donnan potential increases for decreasing ionic strength solutions. For a $(PFS^-/PFS^+)_5$, the top layer PFS^+ introduces more positive charge on the surface ($\omega > 0$). For a high ionic strength solution, it holds: $c_F << c_S$ thus $\Delta\varnothing_D \sim 0$. Under such conditions, extra surface charges can be shielded by the high salt concentration, which shifts the oxidation potential of ferrocene to lower values [33–35].

PFS disassembly profiles were monitored in solutions with different ionic strengths of the electrolyte using cyclic voltammetry (Fig. 3b). In experiments with lower ionic strength of the supporting electrolyte, the PFS multilayers were disassembling faster. Upon oxidation and creation of excess positive charge within the layers, the structures dissolve. The main drive of this process lies in the repulsive electrostatic forces from polymeric domains within the LbL film [22]. Observed differences as a function of ionic strength may be derived from osmotic effects, and longer counterion diffusion distances at lower salt concentrations. Related entropic effects, driven by the lower concentration, may also contribute.

3.3. Counterion effect

To investigate the influence of the ionic structures in the supporting electrolyte on the disassembly profile of PFS LbL systems, different salt solutions were tested. Fig. 4a shows typical cyclic voltammograms recorded with a $(PFS^-/PFS^+)_5$ multilayer on ITO electrode, using different electrolyte solutions. The values of the oxidation potential vary with changes of anions present in the solution. The disassembly profile of $(PFS^-/PFS^+)_5$ bilayers in four

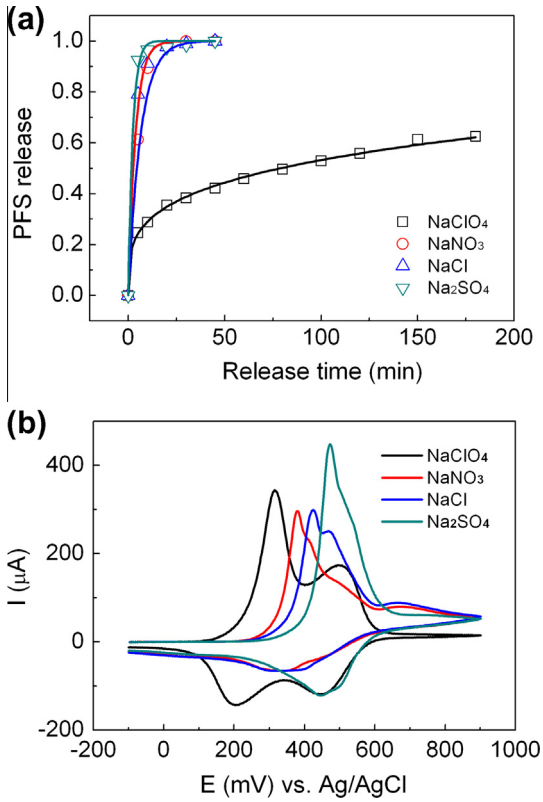

Fig. 4. (a) $(PFS^-/PFS^+)_5$ multilayers dissemble rate as a function of release time at fully oxidation potential of different electrolyte solutions $NaClO_4$ (□), NaCl (○), $NaNO_3$ (Δ), Na_2SO_4 (▽). b) Typical cyclic voltammograms recorded on a $(PFS^-/PFS^+)_5$ multilayer assembled on ITO electrode with different 1 M electrolyte solutions.

different supporting electrolytes ($NaClO_4$, $NaNO_3$, NaCl, Na_2SO_4) of the same molar concentration were compared (Fig. 4b). In NaCl, $NaNO_3$, and Na_2SO_4 electrolyte solution, PFS multilayers were disassembled very fast, with 80% of material released within the first 5 min. However, using $NaClO_4$ electrolyte, it took approximately 5 h to reach complete disassembly.

Interactions of counterions with polyions, and related phenomena, can frequently be correlated with the so-called Hofmeister series [36–38]. The series ranks anions according to the degree of their solvation and follows the order: $ClO_4^- > I^- > NO_3^- > Cl^- > F^- > OH^- > SO_4^{2-}$. On the left side of the series, ions are chaotropic, exhibiting weaker interactions with water. On the right side, ions are cosmotropic, exhibiting strong water solvation. The solubility of anions increases with decreasing hydration entropy ΔH_h according to the Hofmeister series (for ClO_4^- $\Delta H_h \cong -57\ J\ K^{-1}\ mol^{-1}$ and for SO_4^{2-} $\Delta H_h \cong -2000\ J\ K^{-1}\ mol^{-1}$) [39]. The hydration number of anions follows the order $ClO_4^- < NO_3^- \approx Cl^- < SO_4^{2-}$ [40,41]. Since the hydration number differs for every anion, small, hard ions form large water balls and transport large amounts of water with itself due to the high level of solvation [42]. As such, the cosmotropic ions have problems with migration inside multilayers and maintaining proximity of polyelectrolyte domains. On the opposite, perchlorate anions can migrate into the proximity of polyions much faster and compensate their charge in a more localized manner. As a result, upon oxidation, the effective size of charged polymer domains is smaller; thus, the multilayer disassembly is slower (Fig. 4a). We propose that the large difference between perchlorate anions and the other anionic structures in PFS release kinetics is related to ion pairing (complexation) interaction with ferrocium groups. This can be rationalized based on the ionic radius of ClO_4^- and its high polarizability promoting interactions and ion pairing [43–46]. Nishiyama et al. [43] showed the direct detection of ClO_4^- complexes with the ferrocenium moieties using in situ Fourier transform (FT) Raman spectroelectrochemistry. Shimazu et al. [44] presented significant influence of counterions on the ferrocenyl-undecanethiol monolayers structural changes. According to the presented results, the type of anion influences the formation of ionic pair with ferrocenium, and the perchlorate anion is characterized with a particularly high binding constant value [45]. As a consequence, the release rate of the encapsulated guest molecules from the PFS multilayer template is highly dependent on the type of the supporting electrolyte used [47].

3.4. Influence of the polymer molar mass

$(PFS^-/PFS^+)_5$ multilayer films with different molar mass were prepared and LbL assembled on the ITO electrode surface. Three different batches for each PFS^+ and PFS^- were employed, namely 16.7 KD low molar mass (LM), 53 KD medium molar mass (MM), and 250 KD high molar mass (HM). The electrochemical behavior of $(PFS^-/PFS^+)_5$ multilayers was investigated by CV in aqueous electrolytes. Typical cyclic voltammograms are shown in Fig. 5a.

The oxidation peak potentials E_{pc} shifts somewhat toward higher values when the molar mass was increased. (For values of the measured potentials, see supplementary data.) In aqueous solutions, the peak separation $\Delta E_{1/2}$, i.e., the difference between the first and the second oxidation peaks, became smaller with increase in molar mass (for details see supplementary data). $\Delta E_{1/2}$ gives a useful measure of the interaction between the iron centers. This observed effect may be caused by changes in polyion assembly structure on the electrode surface. The use of high molar mass

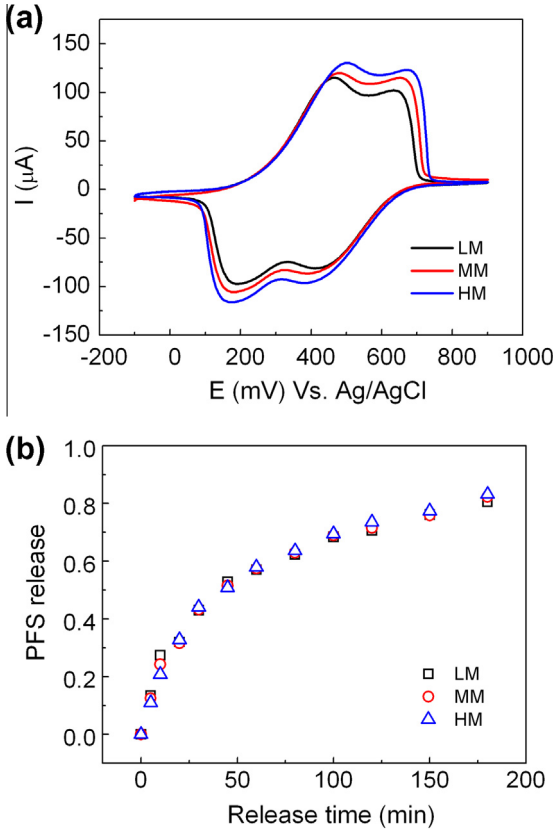

Fig. 5. (a) Typical cyclic voltammograms of $(PFS^-/PFS^+)_5$ with different molar mass, LM, low molar mass (16.7 KD), MM, medium molar mass (53 KD), HM, high molar mass (250 KD), in 0.1 M $NaClO_4$ aqueous solution. (b) Typical disassembly profile of $(PFS^-/PFS^+)_5$ with different molar mass in 0.1 M $NaClO_4$ aqueous solution.

PFS polyelectrolytes is expected to result in assemblies with lower degree of order.

The surface density of the electroactive sites, i.e., ferrocenyl units per area (Γ, calculated from CV, follows: $\Gamma_{LM} = 3.91 \times 10^{-9}$ mol cm^{-2}; $\Gamma_{MM} = 3.97 \times 10^{-9}$ mol cm^{-2}, $\Gamma_{HM} = 4.15 \times 10^{-9}$ mol cm^{-2}. A small increase in the polyion amounts for higher molar mass of the polymer is visible.

PFS multilayer disassembly profiles for different molar masses are shown in Fig. 5b. When polymer molar mass is considered, there are no obvious release rate differences observed.

4. Conclusion

The structure and properties of a new supramolecular nanocomposite based on the LbL assembly of water soluble poly(ferrocenylsilane) polyions are presented. The disassembly of PFS multilayers can be realized electrochemically by prolonged exposure to a small potential. Kinetics and profile of multilayer release can be controlled by blocking layers, surface charge and the type of the supporting electrolyte solution. The discussed phenomena offer insights into structure–property relationships of the assemblies and provide design principles for molecular delivery systems utilizing the disassembly of (PFS^-/PFS^+) multilayers.

Acknowledgments

We are grateful to the A*STAR (Agency for Science, Technology and Research), Singapore and NKTH – A*STAR (Hungarian – Singaporean) Bilateral S&T International Cooperation (BIOSPONA) TeT-08-SG-STAR for providing financial support.

Appendix A. Supplementary material

Supplementary data associated with this article can be found, in the online version, at http://dx.doi.org/10.1016/j.jcis.2013.05.008.

References

[1] D.J. Schmidt, J.S. Moskowitz, P.T. Hammond, Chem. Mater. 22 (2010) 6416.
[2] M.A.C. Stuart, W.T.S. Huck, J. Genzer, M. Müller, C. Ober, M. Stamm, G.B. Sukhorukov, I. Szleifer, V.V. Tsukruk, M. Urban, F. Winnik, S. Zauscher, I. Luzinov, S. Minko, Nat. Mater. 9 (2010) 101.
[3] S. Ganta, H. Devalapally, A. Shahiwala, M. Amiji, J. Controll. Release 126 (2008) 187.
[4] C.M. Jewell, D.M. Lynn, Adv. Drug Delivery Rev. 60 (2008) 979.
[5] D.M. Lynn, Adv. Mater. 19 (2007) 4118.
[6] Y.N. Cui, H.Q. Dong, X.J. Cai, D.P. Wang, Y.Y. Li, ACS Appl. Mater. Interface 4 (2012) 3177.
[7] N.A. Peppas, Y. Huang, M. Torres-Lugo, J.H. Ward, J. Zhang, Ann. Rev. Biomed. Eng. 2 (2000) 9.
[8] D. Jańczewski, J. Song, E. Csányi, L. Kiss, P. Blazsó, R.L. Katona, M.A. Deli, G. Gros, J. Xu, G.J. Vancso, J. Mater. Chem. 22 (2012) 6429.
[9] G. Decher, J.D. Hong, Ber. Bunsen-Ges. Phys. Chem. Chem. Phys. 95 (1991) 1430.
[10] G. Decher, J.B. Schlenoff, Multilayer Thin Film: Sequential Assembly of Nanocomposite Materials, second ed., Wiley-VCH, Weinheim, 2012.
[11] A.S. Abd-El-Aziz, I. Manners, Frontiers in Transition Metal-Containing Polymers, John Wiley & Sons, Hoboken, 2007.
[12] V. Bellas, M. Rehahn, Angew. Chem. Int. Ed. 46 (2007) 5082.
[13] J.C. Eloi, D.A. Rider, G. Cambridge, G.R. Whittell, M.A. Winnik, I. Manners, J. Am. Chem. Soc. 133 (2011) 8903.
[14] Y.J. Ma, M.A. Hempenius, G.J. Vancso, J. Inorg. Organomet. Polym. Mater. 17 (2007) 3.
[15] I.C. Kwon, Y.H. Bae, S.W. Kim, Nature 354 (1991) 291.
[16] K.C. Wood, N.S. Zacharia, D.J. Schmidt, S.N. Wrightman, B.J. Andaya, P.T. Hammond, Proc. Natl. Acad. Sci. USA 105 (2008) 2280.
[17] O. Guillaume-Gentil, N. Graf, F. Boulmedais, P. Schaaf, J. Vörös, T. Zambelli, Soft Matter 6 (2010) 4246.
[18] A.L. Becker, A.N. Zelikin, A.P.R. Johnston, F. Caruso, Langmuir 25 (2009) 14079.
[19] Y.J. Ma, W.F. Dong, M.A. Hempenius, H. Möhwald, G.J. Vancso, Nat. Mater. 5 (2006) 724.
[20] Y.J. Ma, W.F. Dong, E.S. Kooij, M.A. Hempenius, H. Möhwald, G.J. Vancso, Soft Matter 3 (2007) 889.
[21] Y.J. Ma, W.F. Dong, M.A. Hempenius, H. Möhwald, G.J. Vancso, Angew. Chem. Int. Ed. 46 (2007) 1702.
[22] J. Song, D. Jańczewski, Y.J. Ma, M.A. Hempenius, G.J. Vancso, J. Mater. Chem. B 1 (2013) 828.
[23] M.A. Hempenius, F.F. Brito, G.J. Vancso, Macromolecules 36 (2003) 6683.
[24] D. Laurent, J.B. Schlenoff, Langmuir 13 (1997) 1552.
[25] M. Lösche, J. Schmitt, G. Decher, W.G. Bouwman, K. Kjaer, Macromolecules 31 (1998) 8893.
[26] C.C. Moser, J.M. Keske, K. Warncke, R.S. Farid, P.L. Dutton, Nature 355 (1992) 796.
[27] S.S. Isied, A. Vassilian, J.F. Wishart, C. Creutz, H.A. Schwarz, N. Sutin, J. Am. Chem. Soc. 110 (1988) 635.
[28] G.L. Closs, J.R. Miller, Science 240 (1988) 440.
[29] E.J. Calvo, A. Wolosiuk, J. Am. Chem. Soc. 124 (2002) 8490.
[30] F. Caruso, E. Donath, H. Möhwald, J. Phys. Chem. B 102 (1998) 2011.
[31] C. Picart, P. Lavalle, P. Hubert, F.J.G. Cuisinier, G. Decher, P. Schaaf, J.C. Voegel, Langmuir 17 (2001) 7414.
[32] Y.J. Ma, Supramolecular Assembly with Ionic, Redox-Responsive Poly (ferrocenylsilanes): Engineering of Interfaces and Molecular Release Applications. Univ. of Twente, Enschede, PhD thesis, 2008.
[33] M. Tagliazucchi, F.J. Williams, E.J. Calvo, J. Phys. Chem. B 111 (2007) 8105.
[34] M. Tagliazucchi, E.J. Calvo, I. Szleifer, Langmuir 24 (2008) 2869.
[35] M. Tagliazucchi, E.J. Calvo, Chemphyschem 11 (2010) 2957.
[36] F. Hofmeister, Arch. Exp. Pathol. Pharmacol. 24 (1888) 247.
[37] Y. Zhang, P.S. Cremer, Curr. Opin. Chem. Biol. 10 (2006) 658.
[38] H. Fu, X.T. Hong, A. Wan, J.D. Batteas, D.E. Bergbreiter, ACS Appl. Mater. Interface 2 (2010) 452.
[39] Y.J. Zhang, S. Furyk, D.E. Bergbreiter, P.S. Cremer, J. Am. Chem. Soc. 127 (2005) 14505.
[40] J.B. Schlenoff, A.H. Rmaile, C.B. Bucur, J. Am. Chem. Soc. 130 (2008) 13589.
[41] A.G. Volkov, D.W. Deamer, Liquid–Liquid Interfaces: Theory and Methods, CRC Press, Boca Raton, 1996.
[42] R. Zahn, F. Boulmedais, J. Vörös, P. Schaaf, T. Zambelli, J. Phys. Chem. B 114 (2010) 3759.
[43] K. Nishiyama, A. Ueda, S. Tanoue, T. Koga, I. Taniguchi, Chem. Lett. 8 (2000) 930.
[44] K. Shimazu, I. Yagi, Y. Sato, K. Uosaki, J. Electroanal. Chem. 372 (1994) 117.
[45] H.X. Ju, D. Leech, Phys. Chem. Chem. Phys. 1 (1999) 1549.
[46] J. Song, G.J. Vancso, Langmuir 27 (2011) 6822.
[47] J. Song, D. Jańczewski, Y.J. Ma, L. van Lngen, E.S. Ching, Q.L. Goh, J.W. Xu, G.J. Vancso, Eur. Poly. J. (2013), http://dx.doi.org/10.1016/j.eurpolymj.2013.01.029.